JACS JOURNAL OF THE AMERICAN CHEMICAL SOCIETY

Article

Cite This: J. Am. Chem. Soc. 2018, 140, 5069−5076

pubs.acs.org/JACS

Photoswitching of DNA Hybridization Using a Molecular Motor

Anouk S. Lubbe,[†,⊥] Qing Liu,[‡,⊥] Sanne J. Smith,[‡] Jan Willem de Vries,[‡] Jos C. M. Kistemaker,[†] Alex H. de Vries,[‡,§] Ignacio Faustino,[§] Zhuojun Meng,[§] Wiktor Szymanski,[*,†,∥] Andreas Herrmann,[*,‡,#,▽] and Ben L. Feringa[*,†]

[†]Stratingh Institute for Chemistry, University of Groningen, Nijenborgh 4, 9747 AG Groningen, The Netherlands

[‡]Zernike Institute for Advanced Materials, University of Groningen, Nijenborgh 4, 9747AG Groningen, The Netherlands

[§]Groningen Biomolecular Sciences and Biotechnology (GBB) Institute, University of Groningen, Nijenborgh 7, 9747AG Groningen, The Netherlands

[∥]Department of Radiology, University Medical Center Groningen, University of Groningen, Hanzeplein 1, 9713GZ Groningen, The Netherlands

[#]DWI-Leibniz Institute for Interactive Materials, Forckenbeckstr. 50, 52056 Aachen, Germany

[▽]Institute of Technical and Macromolecular Chemistry, RWTH Aachen University, Worringerweg 2, 52074 Aachen, Germany

Supporting Information

ABSTRACT: Reversible control over the functionality of biological systems via external triggers may be used in future medicine to reduce the need for invasive procedures. Additionally, externally regulated biomacromolecules are now considered as particularly attractive tools in nanoscience and the design of smart materials, due to their highly programmable nature and complex functionality. Incorporation of photoswitches into biomolecules, such as peptides, antibiotics, and nucleic acids, has generated exciting results in the past few years. Molecular motors offer the potential for new and more precise methods of photoregulation, due to their multistate switching cycle, unidirectionality of rotation, and helicity inversion during the rotational steps. Aided by computational studies, we designed and synthesized a photoswitchable DNA hairpin, in which a molecular motor serves as the bridgehead unit. After it was determined that motor function was not affected by the rigid arms of the linker, solid-phase synthesis was employed to incorporate the motor into an 8-base-pair self-complementary DNA strand. With the photoswitchable bridgehead in place, hairpin formation was unimpaired, while the motor part of this advanced biohybrid system retains excellent photochemical properties. Rotation of the motor generates large changes in structure, and as a consequence the duplex stability of the oligonucleotide could be regulated by UV light irradiation. Additionally, Molecular Dynamics computations were employed to rationalize the observed behavior of the motor−DNA hybrid. The results presented herein establish molecular motors as powerful multistate switches for application in biological environments.

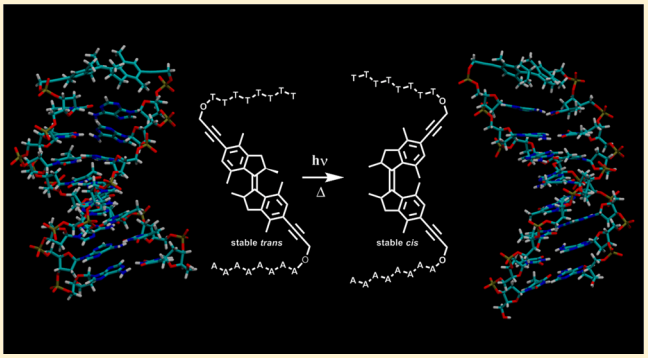

INTRODUCTION

DNA carries the genetic information of all known organisms. In the more than 60 years since Watson, Crick, and Franklin unraveled the double helix,[1] immense advances have been made in our understanding of DNA structure and function. Moreover, the programmable nature of DNA has led to its use in nanotechnology,[2] genetic engineering,[3] information storage,[4] and a range of other applications. In the ongoing search to understand and control the key processes of life, the ability to modulate DNA structure and function is highly desired. Various triggers, such as pH change,[5] small molecules,[6] short primers,[7] biological signals,[8] heat,[9] metal ions,[10] and light,[11−13] have been applied to achieve this goal. The use of light has distinct advantages over the other triggers. Light is noninvasive to living tissue, and a high level of spatial and temporal control over its application is possible.[11] Therefore, light-responsive molecular switches (photoswitches) are considered particularly attractive for reversible control over poly- and oligonucleotide structure and function.[12−15]

In photoregulation of oligonucleotides, extensive use is made of hairpin structures, which comprise short loops of hybridized, self-complementary DNA or RNA. They can form naturally and are frequently found in RNA secondary structure, where, among a variety of functions, they guide folding, protect mRNA from degradation and act as recognition sites or substrates for enzymatic reactions.[16,17] Hairpins are short oligonucleotides and are therefore relatively easy to synthesize, while their self-

Received: September 5, 2017
Published: March 18, 2018

DOI: 10.1021/jacs.7b09476
J. Am. Chem. Soc. 2018, 140, 5069−5076

hybridization is a small-scale model for double-stranded DNA hybridization.[18] Typically in preparing photoresponsive hairpins, the bridging nucleotides of the loop are replaced by a molecular photoswitch.[13] The photoswitch is usually incorporated into the phosphate backbone of the oligonucleotide. In one state, the switch stabilizes the double-stranded helix structure. Irradiation causes a conformational change in the structure of the switch, which leads to destabilization of the helix and a lower melting temperature (T_m). Ideally, in a certain temperature range, the oligonucleotide can be fully switched between double- and single-stranded structures. As a result, in that specific temperature range, the structure can exist as a "closed" double-stranded form, or as an "open" single-stranded form, which may engage in interactions with other biomolecules.

Backbone incorporation of photoswitches was pioneered by Letsinger and Wu,[19,20] using stilbenes as photoactive bridging units; subsequently, this method was expanded with the use of azobenzenes by Yamana and co-workers.[21] Both *trans*-stilbene and *trans*-azobenzene stabilize the hairpins through $\pi-\pi$ interactions with neighboring nucleobases. Upon switching to the nonplanar *cis* isomer, the extra stabilization is lost, leading to a lower T_m. This effect was enhanced by Sugimoto and co-workers, by precise engineering of the azobenzene backbone linker length.[22] In their design (**1**, see Figure 1), the *cis* isomer

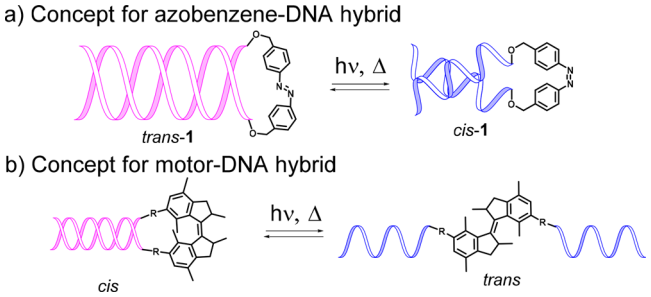

Figure 1. Schematic overview of photoswitchable DNA hairpins. (a) Design by Sugimoto and co-workers based on photoswitchable linker **1**. (b) Concept for linker based on first-generation molecular motors. A full conversion from double-stranded to single-stranded is an unlikely overestimation for both designs, but serves to illustrate the general concept of destabilization through contraction (a) or expansion (b) of the linker.

of the photoswitchable backbone linker is too short to function as a bridgehead for the hairpin. Therefore, the hairpin is distorted upon *trans*-to-*cis* isomerization, leading to additional destabilization and lowering of the T_m. The difference in T_m (ΔT_m) between the two isomers was found to be 20 °C for a 5-base-pair (bp) hairpin (5′-AAAAG-**1**-CTTTT-3′). The ΔT_m is highly dependent on hairpin length, and drops to 17.3 °C when the base pair adjacent to the bridgehead is changed to A-T (5′-AAAAA-**1**-TTTTT-3′) and to 13.9 °C for a 6 bp hairpin (5′-AAAAAA-**1**-TTTTTT-3′).[23] Regardless, by the use of an ingenious linker design, Sugimoto and co-workers were able to achieve an unusually high ΔT_m by the incorporation of only a single molecular photoswitch.[22]

Overcrowded alkene-based rotary molecular motors offer novel opportunities in the field of photoregulation of biologically active molecules due to their unique dynamic properties. The first of this type of responsive molecules was reported in 1999 and was of particular interest because it exhibited repetitive, photochemically driven unidirectional rotation around a carbon−carbon double bond.[24] In recent years, however, molecular motors have found a vast range of applications as multistate switches.[25] The rotary cycle of an overcrowded alkene-based molecular motor consists of four steps and therefore features four different isomers. A detailed description of the rotary cycle and an accompanying scheme can be found in the Supporting Information (SI), in Scheme S1.

The large geometrical changes upon *cis-trans* isomerization in rotary molecular motors, accompanied by the structural rigidity, are particularly suited to induce a significant structural change in a DNA hairpin upon irradiation. Moreover, the four-state switching cycle and the change in helicity of the motor in each rotary step offer potential for new functionalities and a high degree of photoregulation. With this in mind, we set off to evaluate the possibility of using a molecular motor to reversibly control the hybridization of a DNA hairpin (Figure 1b).

We envisioned that one of the isomers (in this case stable *cis*) could be accommodated as a loop element of the hairpin. Upon *cis-trans* isomerization, the motor-bridgehead expands considerably, leading to a destabilization of the hairpin and a corresponding decrease in melting temperature. As a result, at a temperature range around the recorded T_m's, the equilibrium between the DNA double-helical hairpin structure and the single-stranded form could be shifted toward the former, by a photoinduced isomerization from the *cis* form (which should form relatively stable hairpins) to the more destabilized *trans* form. Here, the stable isomers of the motor were synthesized separately to determine the T_m for each isomer after which UV−vis spectroscopy was used to examine the switching behavior of the hybrids.

RESULTS AND DISCUSSION

Computation-Aided Molecular Design of the Linker.

Before starting the synthesis of the target motor−hairpin hybrid, calculations were performed to ensure that the design would be optimal for our envisioned application. By analogy to the azobenzene **1** (Figure 1) reported by Sugimoto and co-workers,[22] we designed a double-primary-alcohol-functionalized motor, which could be incorporated in the DNA strand through standard solid-phase DNA synthesis (SPS). Ideally, the *cis* isomer should have an O−O′ distance of 13.3 Å, which is the optimal bridgehead length. Rigid side chains are necessary to enforce sufficient distortion of the hairpin upon photochemical switching. Our two initially considered designs, linkers **2** and **3**, are depicted in Figure 2. We chose to use first generation motors, which are symmetrical, have limited conformational flexibility, and therefore maximize geometrical change. The xylene-based core structure of these designs has excellent photochemical properties and can be readily synthesized.[26]

Both designs were investigated computationally using Density Functional Theory (DFT; for full computational details see the SI). From these calculations, the potential energy surface (PES) scan of the O−O distance was used to estimate the effectiveness of either possible linker. Figure 3a shows the PES scan for the O−O distance for proposed motor **2**. Because motor **2** has conformational freedom around 4 bonds (highlighted in red in Figure 2), the PES of both isomers is very shallow. There is no obvious global minimum, and a range of distances (7−19 Å for *cis*-**2** (blue squares), 12−20 Å for *trans*-**2** (red circles)) between the terminal oxygen atoms is available to both isomers at no extra energetic cost. At 13.3 Å,

DOI: 10.1021/jacs.7b09476
J. Am. Chem. Soc. 2018, 140, 5069−5076

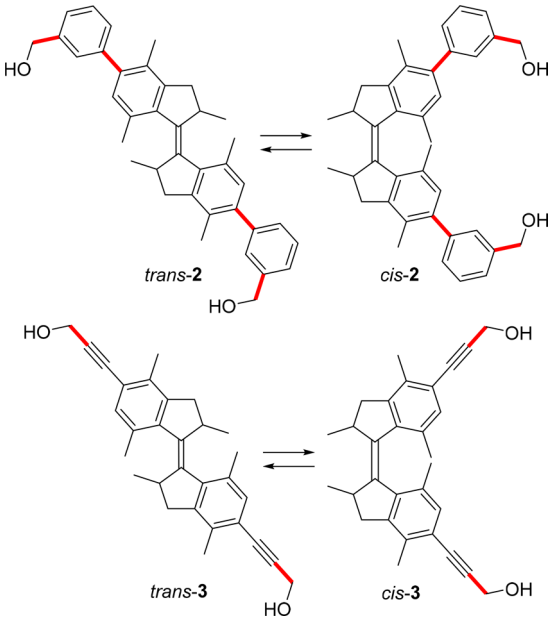

Figure 2. Structures of proposed motor linkers **2** and **3**. The molecules have conformational freedom around the bonds indicated in bold red.[22] Both structures are designed to bring the hydroxy groups closer together upon *trans*-to-*cis* isomerization.

which represents the ideal O−O bridging distance in a hairpin (green line), both isomers can easily be accommodated. Therefore, switching between the two isomers was not expected to result in sufficient destabilization of the hairpin. Figure 3b shows the PES scan for the O−O distance for proposed motor **3**. This structure has much less conformational freedom, which is reflected in a much steeper PES. *cis*-**3** (blue squares) has a global minimum at ∼15 Å. However, the extra energy required to reorganize to an O−O distance of 13.3 Å (green line) is only 1.7 kJ/mol. The *trans* isomer (red circles) has a global minimum at 17.4 Å. Reorganization to 13.3 Å would require an energy input of 22.9 kJ/mol. For comparison, the ΔG of hairpin formation of the entire 5′-TTTTTTTT-X-AAAAAAAA-3′ strand can be estimated at 310 K as 25.5 kJ/mol by using the nearest neighbor model.[27] Therefore, to accommodate *trans*-**3** as a bridgehead in a hairpin, partial disruption of the B-form helical structure by breaking hydrogen bonding between one or more base pairs seems much more likely than distortion of the motor. Based on these computations, we concluded that switching from *cis* to *trans* in a DNA hairpin containing motor **3** as a bridgehead unit will lead to a significant destabilization of the hairpin.

Synthesis of the Molecular Motor-Based Linker 3. The synthesis of *cis*-motor **3** is depicted in Scheme 1, starting from previously reported dibromo-functionalized motor **4**.[28] The preparation of the *cis* isomer is described, but the synthetic route toward the *trans* isomer is identical (see SI, pages S3−S5). Asymmetric synthesis of motor **4** has been performed previously on preparative scale.[28] However, for the sake of synthetic simplicity, we chose to start our investigation using the racemic starting material. The geometric isomers of motor **4** could be separated in this stage through recrystallization and the synthesis of the trans isomer was followed independently. However, in case of the cis isomer, the mixture of isomers was subjected to the next two steps of the synthesis and separation was performed later on. Immediate coupling of **4** to the acetylene moieties was unsuccessful. Therefore, the bromine substituents were converted to iodines in a Finkelstein-type reaction. The coupling to the acetylene unit was initially attempted using propargyl alcohol, however, with poor results. The yield was much improved by using propargyl acetate for the Sonogashira coupling. Protected motor **6** was obtained in 94% yield. At this stage, the *cis* isomer was separated from the mixture of isomers through recrystallization. Motor **6** could be converted into target motor **3** by a base-mediated deprotection in 87% yield. *Trans*-**3** was synthesized in an identical manner, however, a note needs to be added regarding the substitution of the bromine moieties for iodine moieties (**4** to **5**). As this reaction was performed at 130 °C, it caused partial thermal isomerization of *trans*-**5** to *cis*-**5**. After several recrystallization cycles, >95% *trans*-**5** could be obtained and the synthesis was continued using *trans*-**5** in the presence of a small amount of *cis*-**5**.

For incorporation in DNA using solid-phase synthesis, motor **3** had to be converted into the corresponding phosphoramidite building block **8** in two steps (Scheme 1). First, one of the primary alcohols of motor **3** was protected using one equivalent of dimethoxytrityl (DMT) chloride. From this reaction, a 1:2:1 statistical mixture of starting material **3**, monoprotected product **7**, and diprotected motor was obtained, which could easily be separated by column chromatography. The resulting monoprotected motor **7** was relatively unstable and therefore had to be immediately converted into phosphoramidite motor **8**, through coupling with 2-cyanoethyl-*N*,*N*-diisopropylchlorophosphoramidite. This building block was also highly unstable

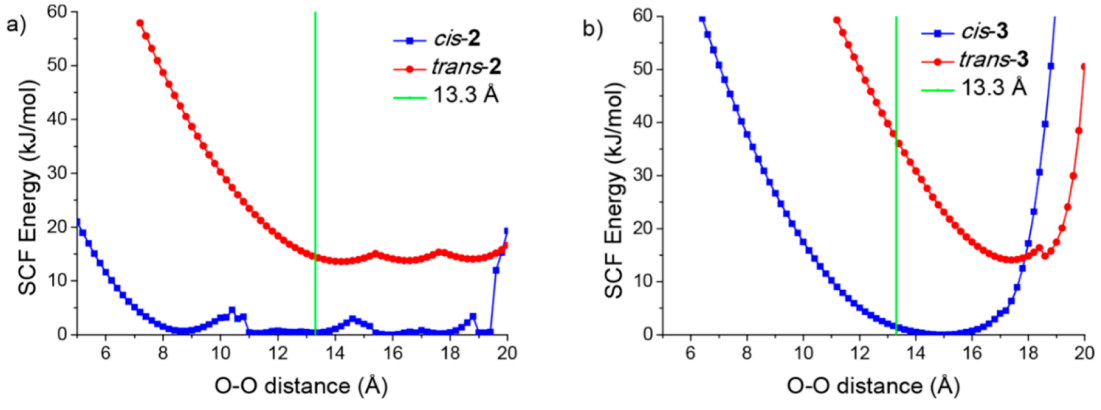

Figure 3. PES scans of the O−O distance in proposed motors **2** and **3**, plotted against the self-consistent field (SCF) energy.

DOI: 10.1021/jacs.7b09476
J. Am. Chem. Soc. 2018, 140, 5069−5076

Scheme 1. Synthesis of Motor 3 and Phosphoramidite Motors *trans*-8 and *cis*-8[a]

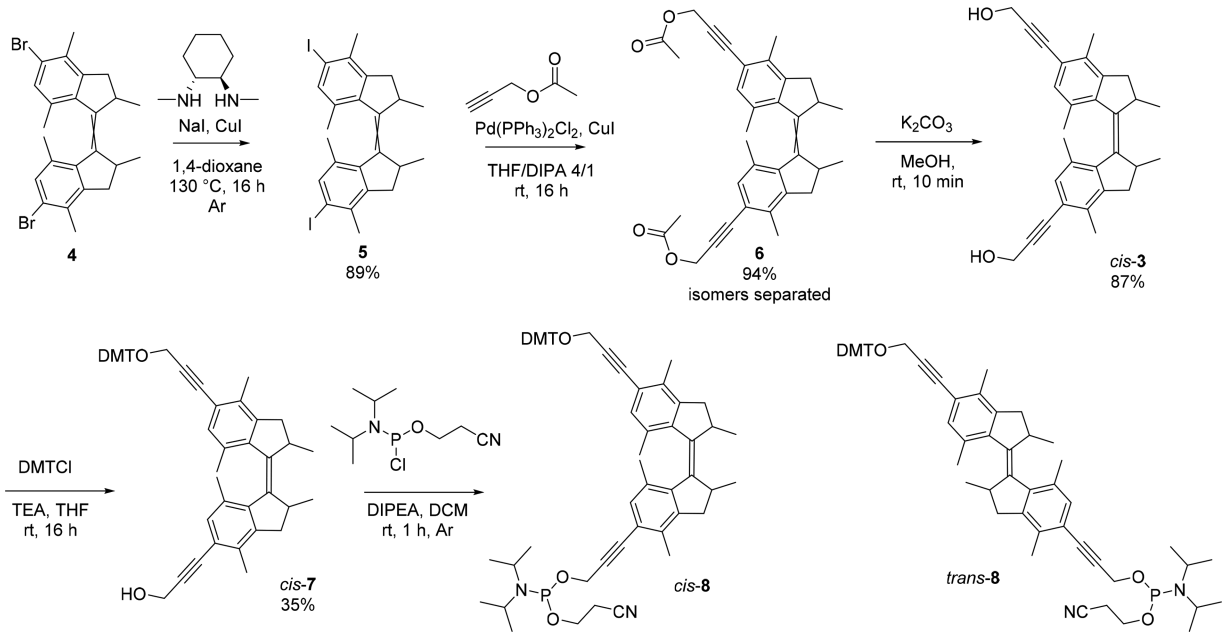

[a]Only synthesis for *cis*-**8** is shown; for *trans*-**8**, see SI, pages S3–S5. Isomers of compound **6** were separated through recrystallization, subsequent yields refer the *cis* isomer only.

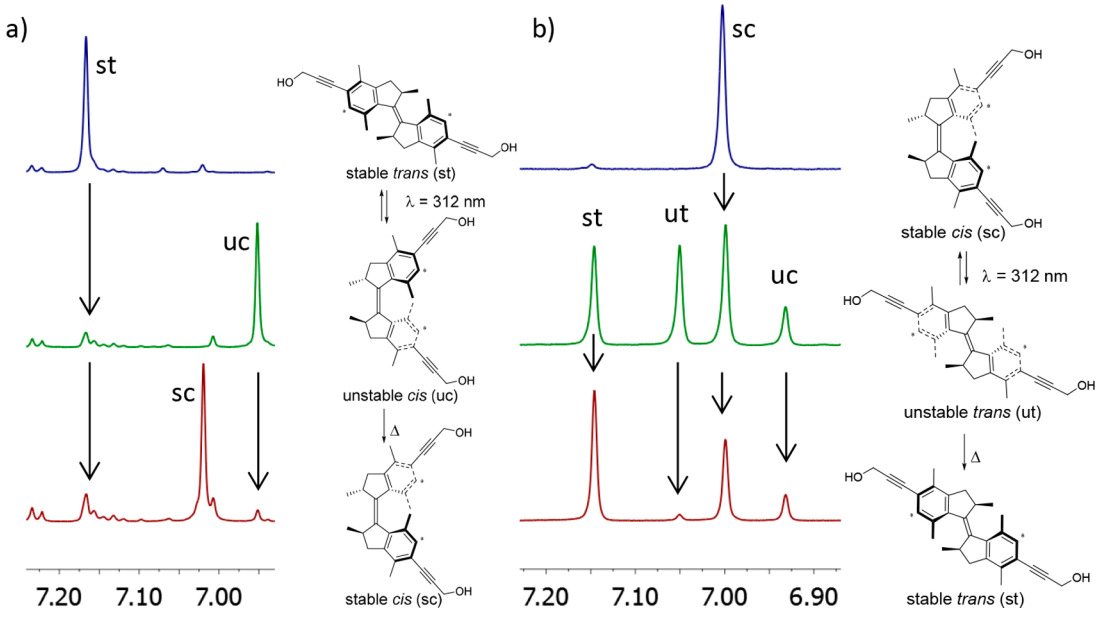

Figure 4. ^{1}H NMR analysis of the rotational cycle of motor **3** (part of spectrum, proton indicated by *). Only aromatic proton depicted for clarity; see Figures S3 and S4 for full spectrum. (a) Stable *trans*-**3** (st) to unstable *cis*-**3** (uc) to stable *cis*-**3** (sc). (b) Stable *cis*-3 (sc) to unstable *trans*-**3** (ut) to stable *trans*-**3** (st). All experiments performed in CD_2Cl_2 (400 MHz, −50 °C).

and was therefore purified by quickly flushing over a SiO_2 column, dissolved in dichloromethane under an argon atmosphere, and immediately used in SPS. ^{1}H and ^{31}P NMR analysis showed that *trans*-**8** contained only 20% product. The main impurity appeared to be a dimer (structure not shown) resulting from a reaction of the starting material **7** and the product **8**, in which the cyanoethyl moiety was replaced by a second motor molecule. As it was established that the hairpin synthesis was not compromised, and to prevent losses by oxidation, a second chromatography was not performed, and this mixture was subjected to SPS. In a similar synthesis for the *cis* isomer of motor-based phosphoramidite **8**, this final step was highly effective, and *cis*-**8** was obtained pure after chromatography.

Photochemistry of the Motor-Based Linker. Prior to SPS of the motor-based hairpin, and to reveal that photoisomerization processes were not compromised, the photochromism and rotary cycle of motor **3** were investigated using UV–vis (see Figure S2) and ^{1}H NMR analysis, revealing excellent photochemical properties. Upon irradiation of stable *trans*-**3** with 312 nm light, a photostationary state (PSS) consisting of 88% unstable *cis* isomer was formed, which

DOI: 10.1021/jacs.7b09476
J. Am. Chem. Soc. 2018, 140, 5069–5076

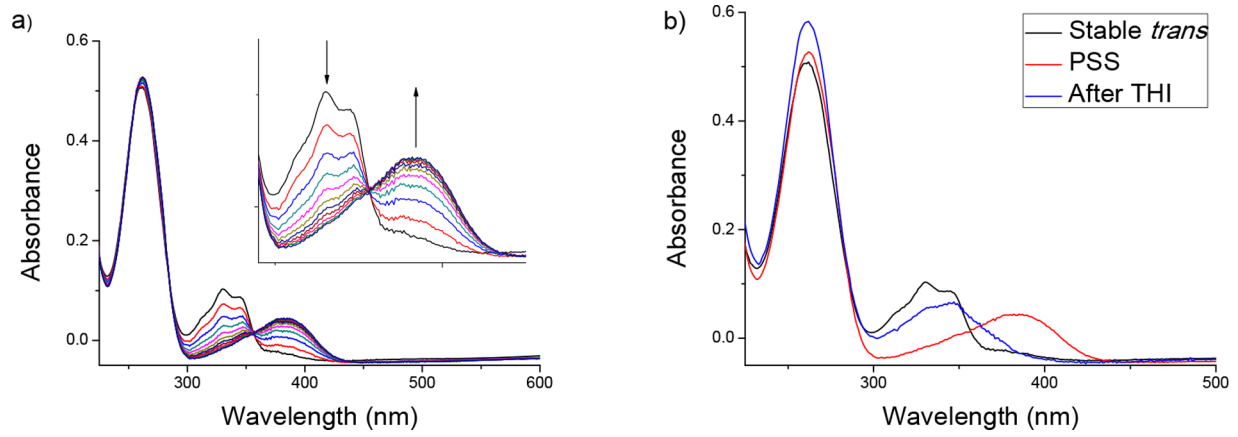

Figure 5. UV−vis spectra of analysis of the photochemical isomerization of stable 8T-*trans*-**3**-8A. (a) Changes of the absorption spectrum of 8T-*trans*-**3**-8A upon irradiation with 312 nm light for 10 min. Spectra were recorded in 1 min intervals. Inset shows the region 290−450 nm. (b) 8T-*trans*-**3**-8A (black line), the sample after irradiation with 312 nm light for 10 min (red line), and the sample after incubation at 67 °C for 6 h (blue line). All spectra recorded in Milli-Q water, 67 °C, ambient atmosphere.

subsequently underwent thermal helix inversion (THI) to stable *cis*-**3** (Figure 4a). No PSS could be observed for the other half of the rotary cycle, since unstable *trans*-**3** readily undergoes THI even at −50 °C, leading to formation of stable *trans*-**3**, which can also undergo photoisomerization to unstable *cis*-**3**. As a result, all four isomers can be observed in the mixture after irradiation (Figure 4b). Using Eyring analysis, the half-life of the unstable *cis* isomer **3** was calculated to be 9.7 h at 37 °C. The half-life of unstable *trans*-**3** was not determined, but is expected to be <1 s at 37 °C, based on our earlier studies of related first generation motors.[26] Therefore this isomer (unstable *trans*-**3**) is of no practical use. For full experimental details, see SI, pages S7−S10.

DNA Synthesis and Melting Point Analysis. Molecular motor building block **8** was introduced into a 16-mer, self-complementary DNA strand using standard solid-phase oligonucleotide synthesis on a DNA synthesizer. *Cis* and *trans* isomers were synthesized separately from stable *cis*-**8** and *trans*-**8**, respectively. The product, 5′-TTTTTTTT-**3**-AAAAAAAA-3′ (8T-**3**-8A), was purified using reversed-phase chromatography followed by anion exchange chromatography. Product identity was confirmed by MALDI-TOF mass spectrometry (Figure S10). Duplex formation of two molecules 8T-**3**-8A was not expected, since this was found to be extremely unfavorable for related oligonucleotides with stilbene backbone linkers.[19] Gel electrophoresis confirmed that both isomers form hairpins (Figure S13). The melting temperature of each hairpin was determined using a SYBR Green I fluorescence assay (Figures S11 and S12). The melting temperature for 8T-*cis*-**3**-8A was determined to be 59 °C, and for 8T-*trans*-**3**-8A to be 65 °C. The ΔT_m is therefore 6 °C, which is a remarkably high value and comparable to the achievement of Sugimoto and co-workers (20 °C/17.8 °C for 5 bp (depending on base pair adjacent to bridgehead), 13.9 °C for 6 bp).[22,23] Comparison with an 8 bp DNA hairpin containing an azobenzene or stilbene linker is not possible. Only three such hybrids were previously reported, and a ΔT_m was not reported for any of them.[29−31] Notably, the T_m of the native hairpin 8T8A was determined to be 51.5 °C. The observation that the T_m of the native hairpin is lower than the T_m of the hybrids can be partly attributed to the fact that the loop in this hairpin consists of a few bases, which are therefore not engaging in base pairing. Typically, a four nucleotide loop is found to be most stable.[32] The loss of two base pair interactions is expected to decrease the T_m a few degrees, while the T_m's of 8T-*cis*-**3**-8A and 8T-*trans*-**3**-8A are, respectively, 7.5 and 13.5 °C higher than the T_m of 8T8A. It seems therefore that for both isomers, the motor has a significant stabilizing effect on the hairpin. A similar stabilizing effect is observed for *trans* azobenzenes and stilbenes, where it has been attributed to π stacking interactions.[12,33]

Motion of the Motor in the DNA Scaffold. For any application under biologically relevant conditions,[34,35] and in this case to achieve photocontrol over DNA secondary structure, it is very important that the switching ability of the motor in the hybrid is retained. To investigate the action of the motor without interaction between the two substituent DNA strands, we started our experiments under non-hybridizing conditions: in Milli-Q water and at 67 °C, above the T_m of either isomer. We subjected a 2.65 μM solution of 8T-*trans*-**3**-8A in Milli-Q to the standard UV−vis experiment used to follow the isomerization processes of a molecular motor (Figure 5). In the initial absorption spectrum (Figure 5a,b, black line) both components of the hybrid can be clearly distinguished. The major absorption band can be attributed to DNA (λ_{max} = 262 nm), while above ∼300 nm, only the motor units contribute to absorption. The band with two maxima at λ_{max} = 330 and 345 nm is characteristic for the stable *trans* conformation of xylene-based first generation motors[26,36,37] and is also observed in the UV−vis spectrum of motor **3** (see Figure S2). Because the DNA does not absorb above 300 nm, the motor unit can be irradiated without affecting the DNA part of the hybrid. Irradiation with 312 nm at 67 °C leads to the appearance of a new absorption band at a higher wavelength (λ_{max} = 385 nm), which typically results from the formation of a higher energy motor isomer (8T-unstable-*cis*-**3**-8A, Figure 5a). The clear isosbestic point indicates the absence of photodamage or side reactions. After 10 min, a photostationary state was reached, and the irradiation was halted (Figure 5b, red line). Subsequently, the sample was left at 67 °C for several hours to induce thermal helix inversion. As expected, the new band disappeared, and an absorption at a lower wavelength (λ_{max} = 347 nm, Figure 5b, blue line) appeared, most likely corresponding to 8T-*cis*-**3**-8A. [We were unable to find separation of the two isomers of 8T-**3**-8A using chromatography, and not enough material was available to attempt characterization through NMR spectroscopy.] MALDI-TOF

DOI: 10.1021/jacs.7b09476
J. Am. Chem. Soc. 2018, 140, 5069−5076

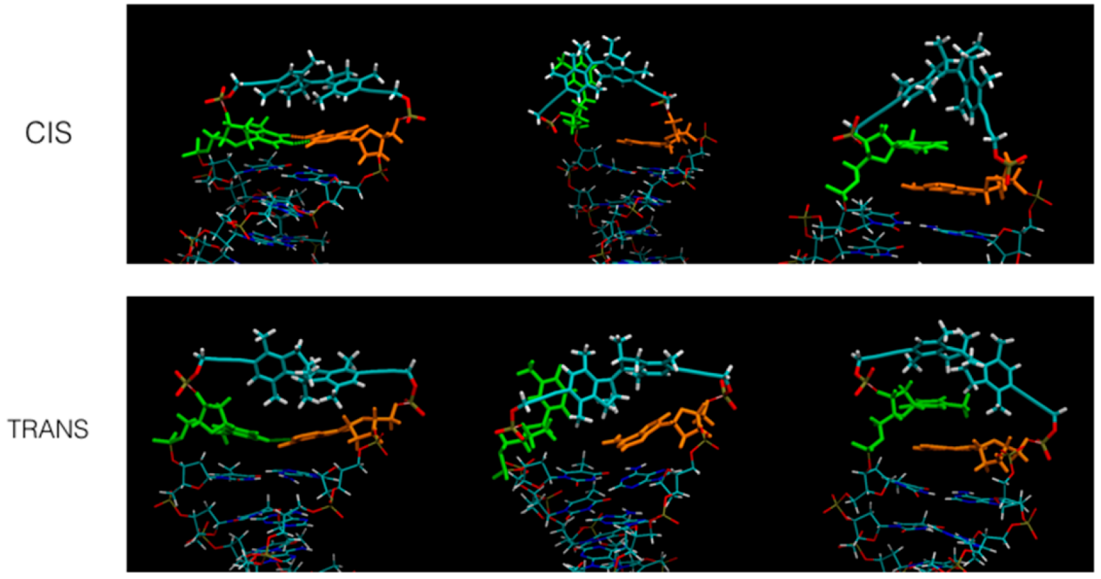

Figure 6. Selected conformations taken from 90 ns MD simulations of hairpin- constructs with the linker in the stable *cis* (top row) and *trans* (bottom row) conformations, respectively. The molecule is visualized using the VMD software, highlighting the switchable bridge (cyan C-atoms). The adenine at the 5′ end is shown entirely in orange and the 3′ thymine in green. H-bonding interactions defined on the basis of the Luzar-Chandler-geometric criterion (donor−acceptor distance within 3.5 Å and donor−H−acceptor angle smaller than 30°) between these two selected base pairs are shown as dashed lines. The leftmost conformation is the starting conformation with a canonical base pairing, obtained after building and briefly equilibrating the model. In the middle, structures in which the thymine base neighboring the switchable bridge flipped out of the hairpin are shown. The rightmost panels show structures in which the base pairs closest to the switchable bridge have stacking interactions instead of base-pairing interaction. In the *trans* form (right bottom), the thymine appears to be interacting also favorably with one of the aromatic moieties of the switchable linker; this interaction is energetically less favorable in the *cis* form.

analysis showed that the hybrid does not undergo degradation (Figure S18). Although the UV−vis spectra alone clearly indicate a photoisomerization followed by THI, the sample used in this experiment was subjected to a melting temperature analysis by a fluorescence assay. We hypothesized that a mixture of the two hairpins (8T-*trans*-**3**-8A and 8T-*cis*-**3**-8A) should lead to two maxima in the differentiated curve of the fluorescence spectrum, corresponding to the two different T_m's. In fact, the main maximum in this curve was found at 59 °C, which corresponds to the T_m of 8T-*cis*-**3**-8A (Figure S16). This result, in combination with the UV−vis spectra depicted in Figure 5, leads us to conclude that an efficient photoisomerization and subsequent THI have taken place. To determine the kinetics of the THI, the absorption of the sample was measured at regular intervals (Figure S14). The half-life of the unstable *cis* isomer of 8T-**3**-8A is determined to be ∼51 min at 67 °C, about 2.5 times slower than for the motor **3** itself (*vide supra*, 19.5 min at 67 °C). Therefore, it appears that motor rotation is slightly slowed down but otherwise unhindered when integrated in the backbone of a biomolecule and operated in aqueous conditions. Because these experiments are performed in bulk solution, irradiation had to be performed for 10 min, and we were unable to look into structural dynamics of the hairpin. However, it may be possible that reconfiguration of the hairpin occurs on a slower time scale than photoswitching of the motor, similar to responses observed in peptides.[38−40] Future investigations may include ultrafast IR studies to elucidate the dynamics of hairpin reconfiguration upon photoswitching.

The experiment was also performed under hybridizing conditions at physiological temperature (37 °C, 20 mM Tris-HCl, 100 mM NaCl, 10 mM $MgCl_2$, pH 8.0). 8T-*trans*-**3**-8A was again readily photoisomerized without the occurrence of side reactions. However, after several hours at 37 °C, only a slight decrease of the absorption band corresponding to the unstable *cis* isomer was observed (see Figure S16). Potentially, helix inversion is hindered by the hybridized DNA strands. A two-dimensional representation of the rotary cycle can give the impression that the THI induces a smaller geometry change to the motor than the photochemical isomerization. However, DFT calculations on the parent xylene-based motor have demonstrated that the THI from unstable *cis* to stable *cis* proceeds through an asynchronous change of the dihedral angle, in which one half is overall rotated approximately 120° with respect to the other half in a combination of backward and forward movement.[41] This asymmetric behavior arises from the steric hindrance between the two halves and could be the reason that for 8T-**3**-8A the THI proceeds less readily than the photochemical isomerization at 37 °C. When the sample was heated to 70 °C (above the T_m), THI occurred in a similar manner in aqueous buffer as in water. For full spectra and MALDI-TOF analysis of the irradiated sample, see SI pages S20−S22. Melting temperature analysis revealed a T_m of 59 °C, indicating efficient conversion to the stable *cis* isomer.

To summarize, the rotational motion of 8T-**3**-8A can be described as follows. Stable 8T-*trans*-**3**-8A forms a hairpin structure with a T_m of 65 °C. Upon irradiation with 312 nm light, photoisomerization to unstable 8T-*cis*-**3**-8A occurs with high conversion. Upon heating, THI can be induced, and stable 8T-*cis*-**3**-8A is formed. The T_m of this isomer is 59 °C, indicating a destabilization of the hairpin structure. To put the measured melting points into perspective, it is important to mention that at the early stages of the project we have targeted the 4T-*cis*-**3**-4A hybrid. However, preliminary melting temperature analysis indicated that the T_m of this compound would be at or around 0 °C. Based on this it was feared that a 5 or 6 bp

DOI: 10.1021/jacs.7b09476
J. Am. Chem. Soc. 2018, 140, 5069−5076

hairpin would also have a T_m below body temperature, and 8T-**3**-8A was targeted instead.

Isomerization from 8T-stable-*cis*-**3**-8A to 8T-stable-*trans*-**3**-8A proved to be challenging due to the very short half-life of the intermediate unstable *trans* isomer (Figure S17). However, we are pleased to report that the photoisomerization and subsequent THI of 8T-stable-*trans*-**3**-8A toward 8T-stable-*cis*-**3**-8A occur without degradation (*vide supra*). Although the elevation to a temperature above the T_m is required to induce THI, the photoisomerization occurs readily under hybridizing conditions and at physiological temperature.

Molecular Dynamics. As discussed above, bridgehead motor **3** was carefully designed to ensure an optimal geometrical change upon *cis-trans* isomerization. We were intrigued to observe that, in sharp contrast to predictions based on our design, 8T-*trans*-**3**-8A proved to have a higher T_m than 8T-*cis*-**3**-8A, since DFT calculations suggested the reverse. However, the DFT calculations were only performed on the motor bridgehead, and artificial contraction was used to simulate a DNA hairpin attached to the oxygen atoms. A DFT study of the full hairpin was not considered feasible, due to the excessive computational time such an investigation would require. To explain the difference in hairpin stability, preliminary Molecular Dynamics (MD) simulations were performed, exploring the conformations that the stable *cis* and *trans* isomers can adopt. The simulations used the well-known AMBER force field for DNA,[42] and that model was extended to include the linker moiety. Native B-DNA hairpin structures were built and bridged by linker **3** in either *cis* or *trans* isomer. Water and counterions were added. Briefly, at 300 K the hairpin was observed to remain largely intact, but in both isomers, the base pair closest to the linker was observed to be able to adopt multiple conformations (Figure 6). These include base-flips and stacking of two bases of the first pair on top of each other, apparently engaging in stacking interactions with one of the aromatic rings of the motor. Selected snapshots from the observed conformations are shown in Figure 6. The simulations allow speculation as to the reasons why the *trans* form of 8T-**3**-8A is more stable than the *cis* form (see caption to Figure 6). For example, stacking interactions between the bases and the motor are possible and are energetically more favorable in the *trans* isomer than in the *cis* isomer, which was further investigated in 1 μs simulations at 333 and 363 K; see SI (pages S23−S30). More extensive simulations should enable us to determine the free energy differences between the different types of conformations and thereby give more insight into the relative stability of the hairpin; investigations that are currently ongoing.

CONCLUSIONS

Aided by computational studies, we have designed a first generation molecular motor-based linker that can function as a photoswitchable bridgehead for an 8-base-pair DNA hairpin. Both *cis* and *trans* isomers of a bifunctional linker were prepared and, after establishing their function as a multistate switch, they were incorporated into a 16-mer strand of self-complementary DNA via solid-phase synthesis. Hairpin formation was confirmed, and the DNA−motor hybrid was shown to be able to undergo both photoisomerization and thermal helix inversion processes. The T_m of 8T-*trans*-**3**-8A was determined to be 65 °C, and the T_m of 8T-*cis*-**3**-8A was 59 °C. An unexpected observation was the destabilization due to *trans-cis* isomerization, since DFT calculations suggested the opposite. However, more extensive MD investigations will provide better insight into the interactions between the hairpin and the photoswitchable bridgehead. The results and structural insights of this study are very important for the design of even more potent molecular motor−backbone linkers. The measured ΔT_m of 6 °C (for an 8 bp hairpin) represents a very promising value which ranks this investigation among the most successful attempts to influence DNA hybridization through the incorporation of a photoswitchable backbone linker. Moreover, the isomerization process was highly efficient, and the bistable switching mode provides a real advance over azobenzenes, for which the thermal *cis−trans* re-isomerization limits possible applications. This study marks the first time that a molecular motor has been used to control the secondary structure of DNA, and in fact one of the first examples of a molecular motor being applied under physiological conditions, demonstrating the ability to regulate a key biological process such as DNA hybridization.

Finally, it must be noted that molecular motors do not just rival conventional photoswitches in efficiency and power. They also offer a much higher degree of control and precision due to their four-state switching cycle and helicity inversion. This investigation has only begun to uncover the vast range of new possibilities that may be accessed in photoregulated biohybrid systems. It is apparent that the motor unit by itself is powerful enough to significantly influence hybridization behavior of short oligonucleotide hairpins. Moreover, our results showcase the potential of rotary molecular motors and consolidate their position among the most effective photoswitches for use in biological surroundings.

ASSOCIATED CONTENT

Supporting Information

The Supporting Information is available free of charge on the ACS Publications website at DOI: 10.1021/jacs.7b09476.

General methods; synthetic procedures; characterization and $^1H/^{13}C$ NMR spectra of all new compounds; explanation of first-generation molecular motor rotary cycle; UV−vis, NMR, and kinetic analysis of rotation of motor **3**; DFT and MD calculations; DNA synthesis; melting temperature analysis; gel electrophoresis; UV−vis and kinetic analysis of motor−DNA hybrid 8T-**3**-8A; and MALDI-TOF analysis of DNA−motor hybrids; and ^1H and ^{13}C NMR spectra of new compounds, including Scheme S1, Figures S1−S22, and Tables S1−S6 (PDF)

MD data (ZIP)

AUTHOR INFORMATION

Corresponding Authors

*w.szymanski@umcg.nl

*a.herrmann@rug.nl

*b.l.feringa@rug.nl

ORCID

Wiktor Szymanski: 0000-0002-9754-9248

Andreas Herrmann: 0000-0002-8886-0894

Ben L. Feringa: 0000-0003-0588-8435

Author Contributions

⊥A.S.L. and Q.L. contributed equally.

Notes

The authors declare no competing financial interest.

DOI: 10.1021/jacs.7b09476
J. Am. Chem. Soc. 2018, 140, 5069−5076

■ ACKNOWLEDGMENTS

We gratefully acknowledge generous support from NanoNed, The Netherlands Organization for Scientific Research (NWO-CW, Top grant to B.L.F. and NWO VIDI Grant no. 723.014.001 for W.S.), the Royal Netherlands Academy of Arts and Sciences (KNAW), the Ministry of Education, Culture and Science (Gravitation program 024.001.035), the European Research Council (Advanced Investigator Grant no. 694345 to B.L.F. and Advanced Investigator Grant no. 694610 to A.H.), and the China Scholarship Council (CSC) for Q.L. and Z.M. We thank Dowine de Bruijn, Dr. S. J. Wezenberg, and Tom van Leeuwen for valuable discussions.

■ REFERENCES

(1) Watson, J. D.; Crick, F. H. C. *Nature* **1953**, *171*, 737−738.
(2) Jones, M. R.; Seeman, N. C.; Mirkin, C. A. *Science* **2015**, *347*, 1260901.
(3) Ledford, H. *Nature* **2016**, *531*, 156−159.
(4) Goldman, N.; Bertone, P.; Chen, S.; Dessimoz, C.; LeProust, E. M.; Sipos, B.; Birney, E. *Nature* **2013**, *494*, 77−80.
(5) Modi, S.; Swetha, M. G.; Goswami, D.; Gupta, G. D.; Mayor, S.; Krishnan, Y. *Nat. Nanotechnol.* **2009**, *4*, 325−330.
(6) Chen, H.; Zhang, H.; Pan, J.; Cha, T.-G.; Li, S.; Andréasson, J.; Choi, J. H. *ACS Nano* **2016**, *10*, 4989−4996.
(7) Zhang, F.; Nangreave, J.; Liu, Y.; Yan, H. *Nano Lett.* **2012**, *12*, 3290−3295.
(8) Douglas, S. M.; Bachelet, I.; Church, G. M. *Science* **2012**, *335*, 831−834.
(9) Gerling, T.; Wagenbauer, K. F.; Neuner, A. M.; Dietz, H. *Science* **2015**, *347*, 1446−1452.
(10) Takezawa, Y.; Shionoya, M. *Acc. Chem. Res.* **2012**, *45*, 2066−2076.
(11) Weissleder, R.; Ntziachristos, V. *Nat. Med.* **2003**, *9*, 123−128.
(12) Szymański, W.; Beierle, J. M.; Kistemaker, H. A. V.; Velema, W. A.; Feringa, B. L. *Chem. Rev.* **2013**, *113*, 6114−6178.
(13) Lubbe, A. S.; Szymanski, W.; Feringa, B. L. *Chem. Soc. Rev.* **2017**, *46*, 1052−1079.
(14) Zhou, M.; Liang, X.; Mochizuki, T.; Asanuma, H. *Angew. Chem., Int. Ed.* **2010**, *49*, 2167−2170.
(15) Liang, X.; Fujioka, K.; Asanuma, H. *Chem. - Eur. J.* **2011**, *17*, 10388−10396.
(16) Bevilacqua, P. C.; Blose, J. M. *Annu. Rev. Phys. Chem.* **2008**, *59*, 79−103.
(17) Svoboda, P.; Di Cara, A. *Cell. Mol. Life Sci.* **2006**, *63*, 901−908.
(18) Yin, Y.; Zhao, X. S. *Acc. Chem. Res.* **2011**, *44*, 1172−1181.
(19) Letsinger, R. L.; Wu, T. *J. Am. Chem. Soc.* **1994**, *116*, 811−812.
(20) Letsinger, R. L.; Wu, T. *J. Am. Chem. Soc.* **1995**, *117*, 7323−7328.
(21) Yamana, K.; Yoshikawa, A.; Nakano, H. *Tetrahedron Lett.* **1996**, *37*, 637−640.
(22) Wu, L.; Koumoto, K.; Sugimoto, N. *Chem. Commun.* **2009**, 1915−1917.
(23) Wu, L.; Wu, Y.; Jin, H.; Zhang, L.; He, Y.; Tang, X. *MedChemComm* **2015**, *6*, 461−468.
(24) Koumura, N.; Zijlstra, R. W.; van Delden, R. A.; Harada, N.; Feringa, B. L. *Nature* **1999**, *401*, 152−155.
(25) Kassem, S.; van Leeuwen, T.; Lubbe, A. S.; Wilson, M. R.; Feringa, B. L.; Leigh, D. A. *Chem. Soc. Rev.* **2017**, *46*, 2592−2621.
(26) Pollard, M. M.; Meetsma, A.; Feringa, B. L. *Org. Biomol. Chem.* **2008**, *6*, 507−512.
(27) SantaLucia, Jr *Proc. Natl. Acad. Sci. U. S. A.* **1998**, *95*, 1460−1465.
(28) Neubauer, T. M.; van Leeuwen, T.; Zhao, D.; Lubbe, A. S.; Kistemaker, J. C. M.; Feringa, B. L. *Org. Lett.* **2014**, *16*, 4220−4223.
(29) Yamana, K.; Yoshikawa, A.; Noda, R.; Nakano, H. *Nucleosides, Nucleotides Nucleic Acids* **1998**, *17*, 233−242.
(30) Yamana, K.; Kan, K.; Nakano, H. *Bioorg. Med. Chem.* **1999**, *7*, 2977−2983.
(31) Lewis, F. D.; Wu, Y.; Liu, X. *J. Am. Chem. Soc.* **2002**, *124*, 12165−12173.
(32) Antao, V. P.; Lai, S. Y.; Tinoco, I., Jr. *Nucleic Acids Res.* **1991**, *19*, 5901−5905.
(33) Lewis, F. D.; Liu, X.; Wu, Y.; Miller, S. E.; Wasielewski, M. R.; Letsinger, R. L.; Sanishvili, R.; Joachimiak, A.; Tereshko, V.; Egli, M. *J. Am. Chem. Soc.* **1999**, *121*, 9905−9906.
(34) Poloni, C.; Stuart, M. C. A.; van der Meulen, P.; Szymanski, W.; Feringa, B. L. *Chem. Sci.* **2015**, *6*, 7311−7318.
(35) García-López, V.; Chen, F.; Nilewski, L. G.; Duret, G.; Aliyan, A.; Kolomeisky, A. B.; Robinson, J. T.; Wang, G.; Pal, R.; Tour, J. M. *Nature* **2017**, *548*, 567−572.
(36) Wang, J.; Hou, L.; Browne, W. R.; Feringa, B. L. *J. Am. Chem. Soc.* **2011**, *133*, 8162−8164.
(37) Zhao, D.; Neubauer, T. M.; Feringa, B. L. *Nat. Commun.* **2015**, *6*, 6652.
(38) Bredenbeck, J.; Helbing, J.; Sieg, A.; Schrader, T.; Zinth, W.; Renner, C.; Behrendt, R.; Moroder, L.; Wachtveitl, J.; Hamm, P. *Proc. Natl. Acad. Sci. U. S. A.* **2003**, *100*, 6452−6457.
(39) Ihalainen, J. A.; Bredenbeck, J.; Pfister, R.; Helbing, J.; Chi, L.; van Stokkum, I. H. M.; Woolley, G. A.; Hamm, P. *Proc. Natl. Acad. Sci. U. S. A.* **2007**, *104*, 5383−5388.
(40) Regner, N.; Herzog, T. T.; Haiser, K.; Hoppmann, C.; Beyermann, M.; Sauermann, J.; Engelhard, M.; Cordes, T.; Rück-Braun, K.; Zinth, W. *J. Phys. Chem. B* **2012**, *116*, 4181−4191.
(41) Pérez-Hernández, G.; Gonzaléz, L. *Phys. Chem. Chem. Phys.* **2010**, *12*, 12279−12289.
(42) Lindorff-Larsen, K.; Piana, S.; Palmo, K.; Maragakis, P.; Klepeis, J. L.; Dror, R. O.; Shaw, D. E. *Proteins: Struct., Funct., Genet.* **2010**, *78*, 1950−1958.

DOI: 10.1021/jacs.7b09476
J. Am. Chem. Soc. 2018, 140, 5069−5076